Geophysical Journal (1988) **95**, 561–577

Lateral variation of upper mantle structure beneath New Caledonia determined from *P*-wave receiver function: evidence for a fossil subduction zone

Marc Regnier
ORSTOM, BP A5, Noumea cedex, New Caledonia

Accepted 1988 June 8. Received 1988 June 8; in original form 1987 December 2

SUMMARY

Short-period teleseismic *P*-waves recorded at Noumea, New Caledonia, from intermediate and deep focus earthquakes in SE Asia and the SW Pacific are used to investigate crustal and upper mantle structure of the Norfolk ridge, which is currently described as a zone of convergence in its caledonian part. Radial components recorded from various source back-azimuths show a succession of large *P*-to-*S* converted waves whose timing and polarity suggest the presence of a north-dipping low-velocity zone at approximately 60 km depth below the station. The inferred strong lateral variations of structure in the upper mantle are also supported by observations of complex horizontal particle motions and large tangential components which exhibit clear *P*-to-*S* phases. The high velocity contrast observed across these dipping interfaces is interpreted as a structural remnant of the New Caledonia basin oceanic crust which would have been underthrust beneath the New Caledonia crust. Using geometrical ray theory in dipping structure, a model valid for the Noumea station has been derived. The crust is apparently quite homogeneous. It is 26 ± 1 km thick beneath the station and seems to thicken eastward as deduced from the orientation of the Moho. The low average crustal velocities suggest a continental nature for New Caledonia. Toward the thrust zone, the Moho is a thick transition zone whereas it can be modelled by a sharp boundary elsewhere. The inferred structure can be interpreted in terms of either a dead subduction zone or an underthrusting zone. According to the history of compressive deformations observed in land, the underthrusting would likely have been syntectonic of the New Caledonia late Eocene obduction.

Key words: crustal and upper mantle structure, 3-D synthetic seismograms, fossil subduction zone

INTRODUCTION

Characterization of island crust and upper mantle is of major importance in understanding its processes of formation and solving related tectonic problems. In previous studies (e.g. Zucca, Hill & Kovack 1980; Ibrahim *et al.* 1980), island structures have been found to be complex and to depart strongly from a flat layered model. The tectonic history and previous geophysical studies of New Caledonia suggest that this might also be the case for this island.

It is now well known that the analysis of receiver function provides an inexpensive and efficient method of constraining deep structure parameters that other methods cannot measure. Where complex structure is expected, 3-D modelling (Langston 1979, 1981) may yield a more realistic geological model. In this study, short-period waveform data from the three-component station NOU (Noumea) of the ORSTOM network in New Caledonia are examined to investigate crustal and upper mantle structure beneath the station. Aside from the geodynamical context, this work was also motivated by the observation of a striking difference between the two horizontal components for teleseismic events. Indeed, in all cases, a significant tangential *P*-wave has been observed. Synthetic seismograms show that the most characteristic feature of longitudinal body-wave propagation in laterally varying media is the existence of a tangential *P*-wave with azimuthally dependent amplitudes and timing (Langston 1977a). First, these observations are used to estimate the orientation and the dip of the major interfaces under the station. As usual, depth and velocity contrast are mainly determined from the deconvolved radial component. In a second step, the best deconvolved data are modelled by 3-D geometrical ray tracing (Langston 1977a; Sorrels, Crowley & Veith 1971). In our computation, the discontinuities of the structure are simply described by planar interfaces. Only some of the observed phases can be considered as correctly modelled in our study, mainly the direct ones, due to the limitation of the planar assumption

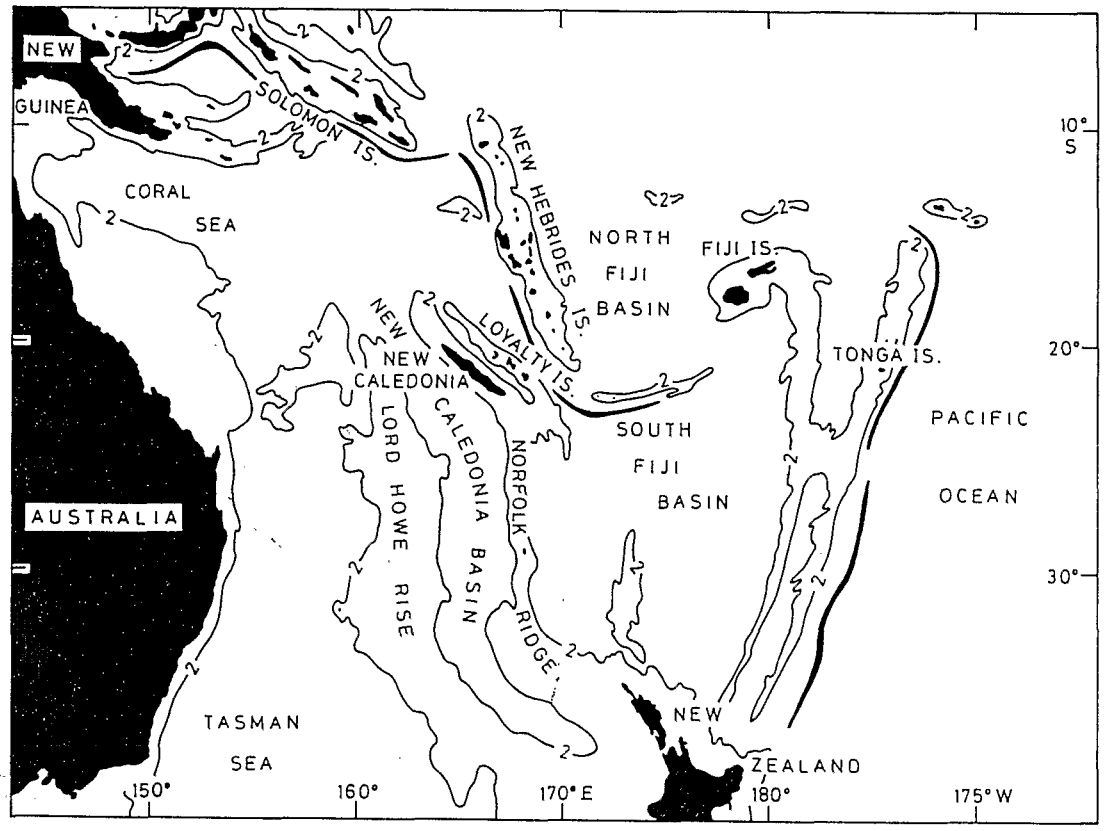

Figure 1. Location of New Caledonia in the SW Pacific.

which is certainly not valid over great distances and which breaks down in the case of a multi-reflected ray path in the crust. Using a short-period system, we may expect good timing and good crustal resolution. Matching amplitudes, on the other hand, is a rather severe problem in this period range where frequency-dependent effects such as attenuation or geometrical spreading effects at irregular interfaces can occur.

The purpose of this study was initially to estimate some parameters of the crust such as its thickness, its mean velocities and density, and also to check if any slope on the Moho could be observed. At greater depth we have found some unusual layered structures characterized by strong lateral variation. Solutions to the geodynamic problem posed by this group of dipping layers will be discussed with the problem of the topography and the thickness of the Moho transition zone.

THE GEOLOGICAL SETTING

The island of New Caledonia, located just north of the Tropic of Capricorn, is part of the Norfolk ridge. This aseismic ridge belongs to the Indo-Australia plate, and spreads out between the New Hebrides island arc and the north island of New Zealand (Fig. 1). New Caledonia is the emergent part of an 800 km long structure oriented NW–SE whereas the southern half of Norfolk ridge trends N–S. Until Cretaceous times, this ridge was the eastern margin of the Australian–Gondwana continent (Paris & Lille 1977; Packkam 1982). It was then rifted eastward by the opening of the New Caledonia basin in late Cretaceous (Hayes & Ringis 1973; Falvey & Mutter 1981). An important geologic feature of New Caledonia is the presence of an ophiolite nappe which outcrops along the length of the island. It ends abruptly along the southeastern coast, and as klippen distributed along the northwestern coast (Fig. 2). Collot, Misseque & Malahoff (1982) have established, using gravity and refraction data (Pontoise *et al.* 1982), that this large ultramafic exposure, a consequence of upper Eocene obduction (Paris 1981), is rooted eastward in the West Loyalty basin. They also show, from the asymmetry of transverse gravity profiles across the island, that the crust of the island thickens eastward. It reaches 30 km under the West Loyalty basin, where the upper crustal layers are well defined by off-shore seismic refraction and reflection profiles. Similar crustal thicknesses were also obtained by Dubois (1971) from the analysis of travel-time residuals at NOU and body-wave velocity around New Caledonia. He found that the Moho lies at a depth of 36 km under the central mountain chain and rises westward to 20 km depth under Noumea. The station NOU is on an upper Eocene sedimentary sequence, which is part of a long narrow folded and thrusted sedimentary belt lying along the southern half of the western coast. In the surrounding area, refraction profiles in the Loyalty basin (Pontoise *et al.* 1982) and in the New Caledonia basin (Shor, Kirk & Menard 1971) show normal oceanic crust but with a thick sedimentary upper layer. This has been explained (Dubois *et al.* 1974) by the large amount of mafic and ultra-mafic material provided by the erosion of the uplifted peridotitic sheet covering the continental body of New Caledonia island (Paris 1981).

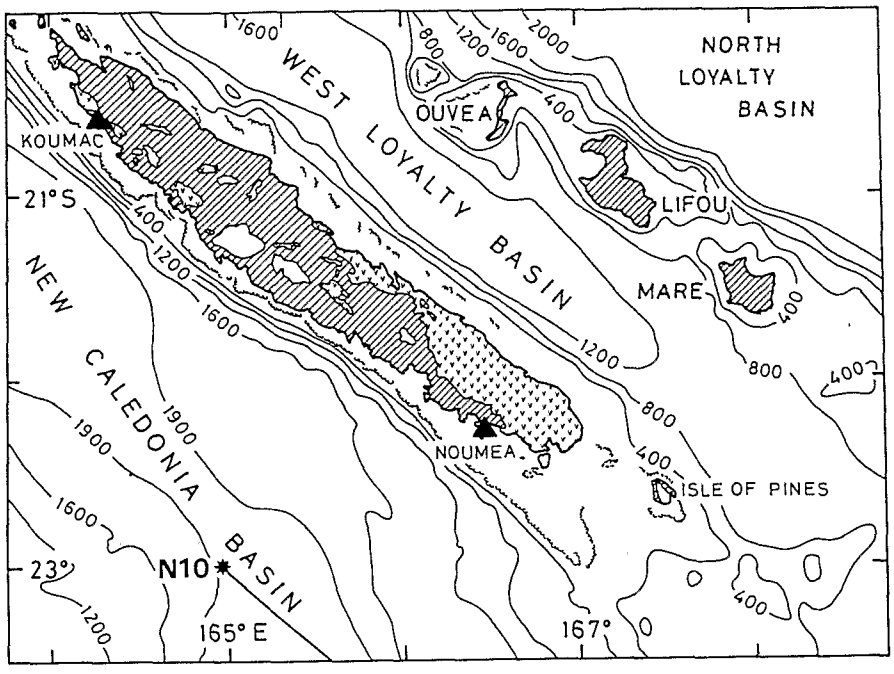

Figure 2. Simplified geological map of New Caledonia after Paris (1981). Bathymetric contours are in fathoms. The *V*-filled areas represent the ultramafic complex. The solid triangles show the location of the Noumea station (NOU) and Koumac station (KOU). The stars indicate refraction profiles.

Very little is known concerning the upper mantle beneath the island. Using travel-time residuals, Dubois *et al.* (1973) and Poupinet (1977) showed that the upper mantle is slower northeastward and faster westward. Dziewonski & Anderson (1983), after inversion of a very large data set, give station corrections on a worldwide scale. Their results for NOU confirm those previous observations. They give an azimuth of N 5° for the slow direction, which is again northward. From their observations, Dubois *et al.* (1973) and Poupinet (1977) conclude with opposite models. The former author, using geological data, argues for a NE dipping low-velocity zone, while, the latter one, by analogy with travel-time residual patterns of active island arcs, suggests that the low-velocity zone should dip in the opposite direction.

THE DATA

Unfortunately, digital recording was not available at NOU for the events processed in this paper. The new Geoscope station of Noumea (Romanowitz *et al.* 1984) is now operating at a quieter site and is starting to provide high quality digital data in several frequency bands. The short-period seismometers used for the present study may be fairly well compared with the analogue short-period instruments of the World Wide Standard Seismograph Network (WWSSN). The magnification is 11000 at 1 Hz ($T_s = 1.1$ s and $T_g = 0.5$ s). The instrumental transfer function is shown in Fig. 3. It has been computed from the actual values of the instrumental parameters measured during a calibration check. The recording paper speed is 60 mm min^{-1}. For digitizing purposes, the records were enlarged to simulate a paper speed of 120 mm min^{-1}. The smallest sampling interval was 0.1 mm and the sampling was made in unequal increments with about 7 or 8 points/s. The hand-digitized data were linearly interpolated at a constant time spacing. Fig. 4 shows three examples of teleseismic *P*-wave data with the vector rotation of the horizontal components into the theoretical ray back azimuth to obtain radial and tangential motions. To span a large azimuthal variation, 15 events were selected according to the criteria: a good signal-to-noise ratio and a simple waveform on the vertical component. This last condition was not always fullfilled due to the use of short-period records where the

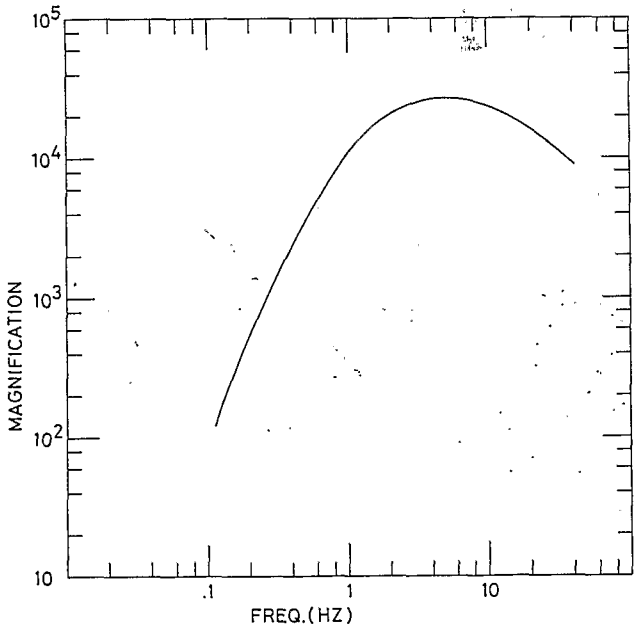

Figure 3. Amplitude displacement response curve of the seismograph system at NOU.

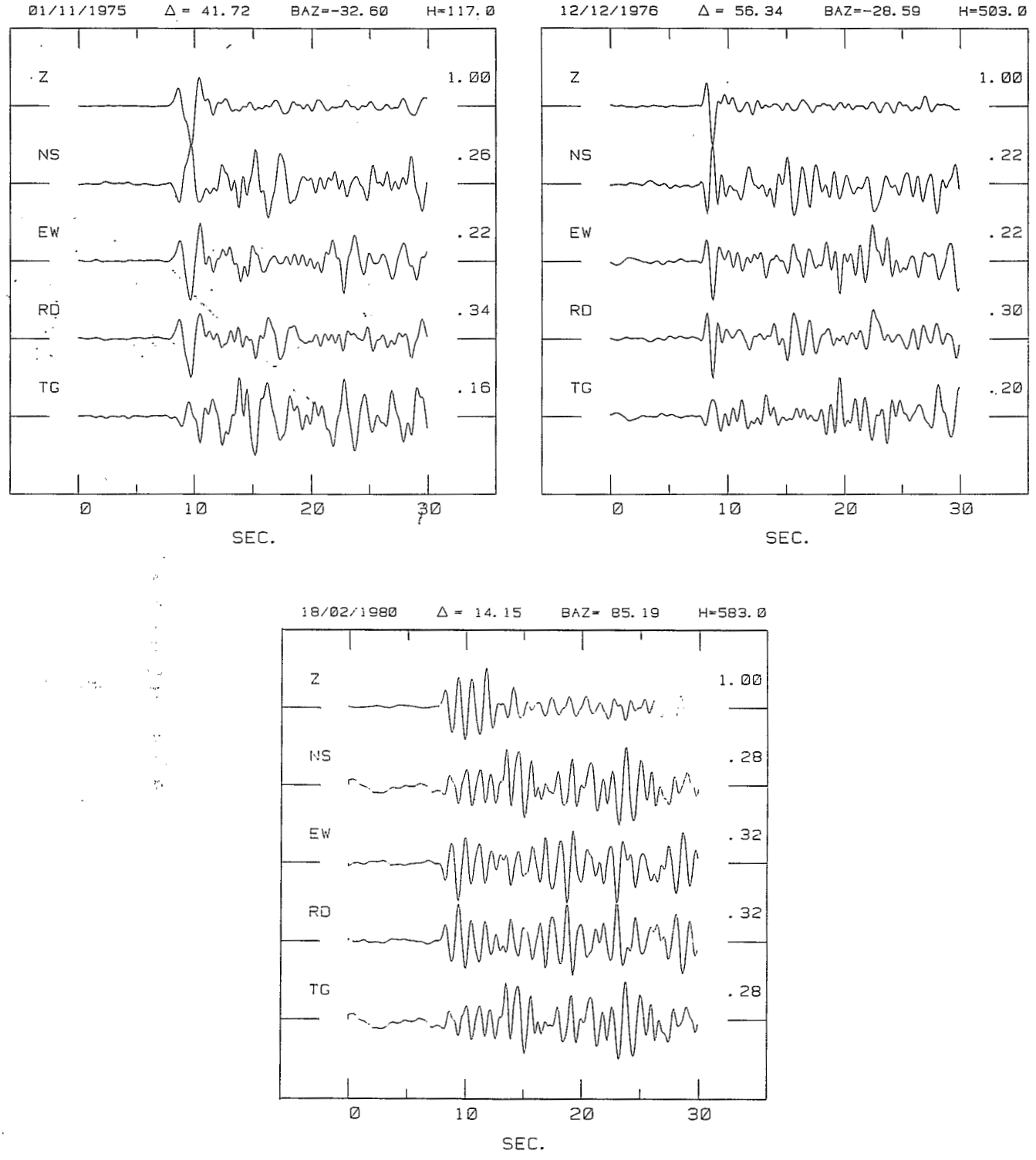

Figure 4. Examples of observed teleseismic *P*-waveform data recorded at NOU. Z, NS, EW, RD and TG are the vertical, north–south, east–west, radial and tangential components of ground motion, respectively.

apparent duration of the source time function is often greater than 2 or 3 s for large events. As far as possible, we tried to find deep events to avoid multiple phases in the source time function. Unfortunately, no earthquake was found in the SW quadrant. Because of the low magnification of the instrument and the location of Noumea with respect to South American seismic zones (distances >100°), events selected to the east of NOU have short epicentral distance (distances <20°). They are mainly deep focus earthquakes of the Tonga–Kermadec subduction zone. Parameters of events used in this study are listed in Table 1.

Considering the waveforms shown in Fig. 4, we must

Table 1. Event parameters (ISC).

Date	Latitude, Longitude (deg.)	H (km)	Mb	D (deg.)	BAZ (deg.)	Location
4/2/65	27.23 S, 179.02 W	401	4.5	14.08	113.29	Kermadec
9/7/74	9.80 S, 108.49 E	60	6.0	56.77	272.79	Java
11/1/75	13.82 N, 144.79 E	117	6.0	41.72	327.4	Marianas
12/21/75	51.93 N, 151.57 E	546	6.0	75.06	350.53	Okhotsk
12/12/76	28.04 N, 139.67 E	503	5.8	56.34	331.41	Bonin
6/17/77	19.85 S, 179.10 W	673	5.6	13.71	82.37	Tonga
11/21/77	29.46 S, 178.90 W	329	4.9	14.98	121.40	Kermadec
12/23/78	23.17 N, 122.00 E	47	6.5	62.57	313.44	Taiwan
5/13/79	19.00 N, 145.42 E	256	5.9	45.92	331.79	Marianas
7/24/79	17.59 S, 178.80 W	538	5.3	14.64	73.92	Toga
10/12/79	46.54 S, 165.91 E	33	6.0	2.18	180.90	New Zealand
12/11/79	28.95 N, 140.94 E	126	6.2	56.58	333.12	Bonin
2/18/80	20.43 S, 178.50 W	583	5.4	14.15	85.19	Tonga

emphasize the important difference between the N–S and E–W components in the first 10 s of the record following the direct wave. In flat-lying structure, scattered *P*- and *SV*-waves will be confined in the vertical ray plane and therefore the tangential component will always be zero. It follows that the N–S and E–W components will be homothetic with a constant amplitude ratio for a given ray parameter. On the contrary, the signal on the tangential component at NOU is largely above the noise level and many of its phases can be easily correlated with those existing on the radial component or on the N–S and E–W components. Fig. 5 shows normalized horizontal particle motion diagrams for two of the events of Fig. 4. We can see a first direction of motion, i.e. the direct compressional wave, mostly radial with little energy deflected into the tangential direction, while the following P_s converted waves are in the tangential direction of motion as well as in the radial direction. We are clearly faced with a 3-D problem when looking at the structure under Noumea.

COMPUTATION OF SYNTHETIC SEISMOGRAMS

To resolve the structure beneath Noumea, we have used a waveform matching technique with 3-D synthetic seismograms computed with the method proposed by Langston (1977a). The structure under the station is described by homogeneous layers with horizontal or dipping planar interfaces. A dipping interface is defined by its dip and strike. Waveform modelling with ray tracing synthetic seismograms has been commonly performed for long-period seismograms. The number of phases to compute is then quite small due to the poor resolution for the long wavelength used. In the short-period case, many more multiples and conversions have to be computed, as done in the exact solution of the Thomson–Haskell method, to get a good fit with data. In our procedure, for a ray made of N segments, all the possible combinations of compressional or shear velocities in each layer, i.e. $2^{**}N$, can be computed and all the possible ray geometries including up to two reverberations per layer or per group of layers can be computed. In practice, this procedure has been found to be time consuming, especially due to the number of conversions. The number of conversions was finally reduced to two for a ray travelling in the model without loss of quality in the synthetic seismograms. Fig. 6 shows examples of synthetics for model 1 listed in Table 2 with all the dips set to zero. The computed impulse responses have been convolved with an incident wavelet taken from the vertical *P*-waveform of the 1975 December 12 event. The first row is computed using a propagator matrix method (Haskell 1962), and the second row with our ray tracing program. These traces are almost identical during the first ten seconds. They differ only slightly later in the coda. To illustrate our choice of the number of conversion, we display in the third row of Fig. 6 a set of synthetics computed with the same ray geometry as above, allowing now only one *P*-to-*S* conversion per arrival over the whole ray length. This example is still acceptable and gives us a lower bound of quality for our synthetic calculation.

The synthetics on Figs. 7 are computed using model 1 (Table 2) for back-azimuths varying from −90° to 90°. Tangential waveforms with large relative amplitudes are now set up within the 3-D model and give the most obvious signature of the geometric complexity of the structure. In these examples, the information on the geometry of the inclined plane could be deduced from both waveform and relative arrival times of converted phases in the short-period range. Indeed, the arrival time of the *PS* low-velocity zone (LVZ) phases increase by more than 1 s when passing from the strike direction (−90° or 90°) to the dip direction (10° to −10°). This difference can be used to constrain the orientation of the interface together with the antisymmetric behaviour of the corresponding tangential phase. Note that, in the case of our particular model, the tangential first motion is mainly controlled by Moho orientation.

DATA ANALYSIS

First we extracted information about the strike and the dip of sharp discontinuities existing in the structure from the polarity of the tangential *P*-wave versus back-azimuth. As the tangential first motion is often poorly emergent from the noise, it was safer to read it directly on the original seismogram instead of using the deconvolved traces which are presented below. Fig. 8 shows a polar plot of sign change between radial and tangential first motion versus back-azimuth. A plus sign means that the tangential has the same polarity as the radial, a minus sign, the opposite

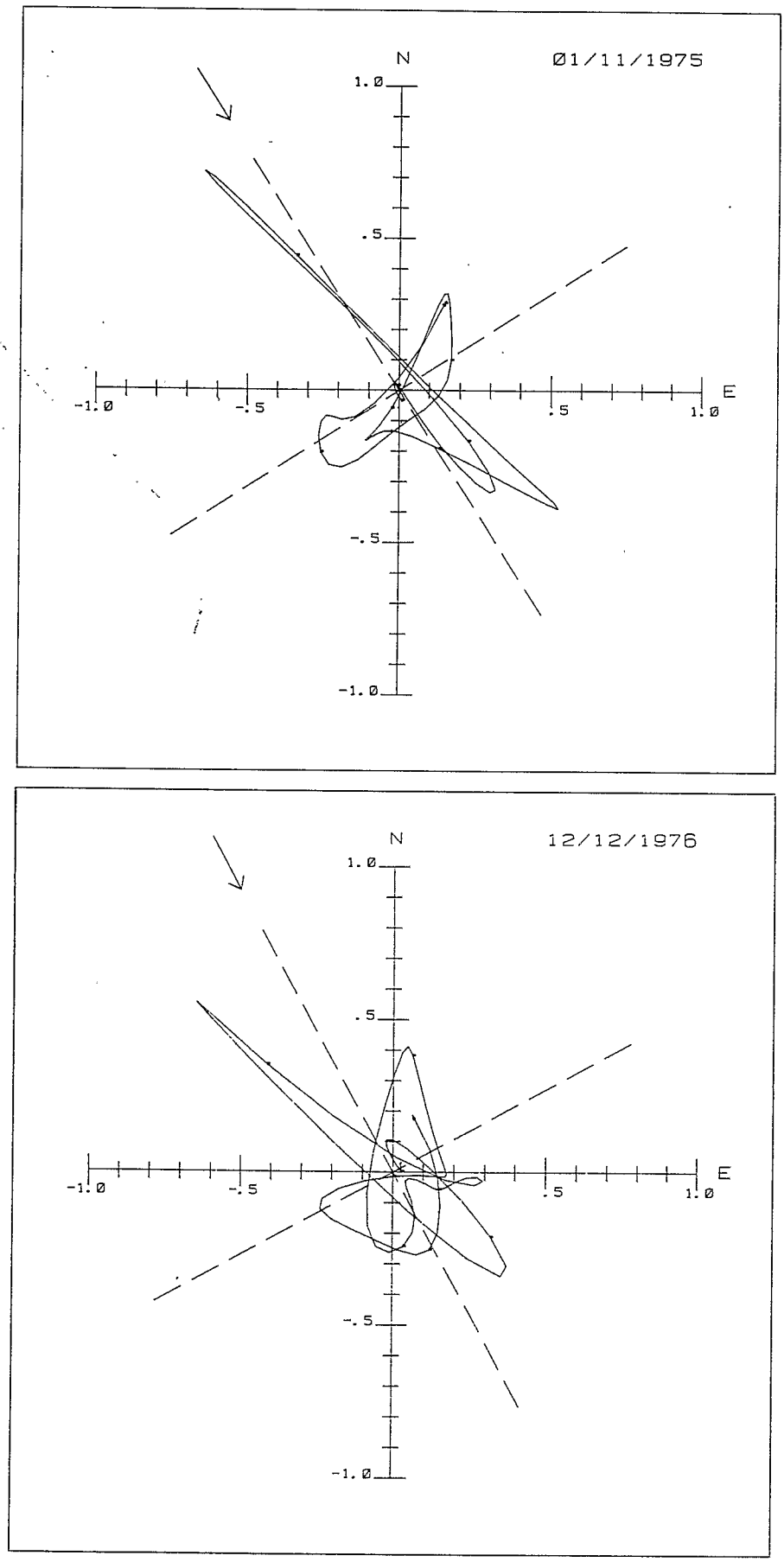

Figure 5. Plot of the first 7 s of the horizontal particle motion for the events shown in Fig. 4. The arrow indicates ray approach back-azimuth.

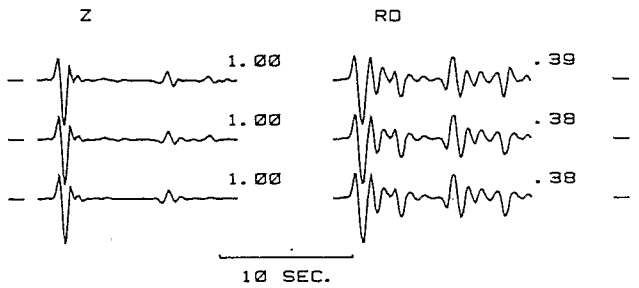

Figure 6. Comparison of synthetics derived from Haskell matrix method (top) our ray tracing method with two (middle) and one (bottom) conversions, respectively, allowed per arrival during the ray propagation in the model. The input waveform used to make all the synthetics was taken from the 1976 December 12 event (Fig. 4). A ray parameter of 8 s/deg. is assumed in the computation.

polarity. Around the plot the original vertical, radial and tangential data are shown. According to computed polarities in dipping structure, the plot efficiently constrains a global dip azimuth to N 90° ± 4°. However, the horizontal relative amplitude variation does not show the corresponding pattern, which would be a tangential amplitude decreasing toward both the dip and opposite azimuth. This may be partly due to differences between horizontal instrumental responses, but must principally reflect the complexity of the structure which cannot be resolved by this plot for every interface geometry.

In order to compare horizontal components, it is necessary to remove path and source effects which are different from event to event. For that purpose, an equalization procedure, introduced by Helmberger & Wiggins (1971) and adapted by Langston (1979), is used. It allows us to deconvolve the vertical component, regarded here as a good estimate of the source function, from the horizontal components in a stable process. This technique, which performs the division of the Fourier transform of the horizontal component by that of the vertical component, involves two parameters, a and c. They control (respectively) the width of the Gaussian spectral window which excludes high-frequency noise in the final frequency band of the horizontal response and the minimum allowable spectral amplitude of the vertical component in the spectral division. The impulse response is obtained by transformation back into the time domain. In our case, $a = 3$ and $c = 0.01$ for all the estimated radial and tangential impulse responses presented here. The width of the gaussian is chosen to produce a pulselike time function of approximately 0.8 s duration which is close to the apparent period of the vertical P-waveform. For more details and explanation, see Langston (1979) or Owens, Zandt & Taylor (1984).

Table 2. Structure models.

Layer	V_p (km/s)	V_s (km/s)	g (gm/cm^3)	Th. (km)	Strike (deg.)	Dip (deg.)
Model of New Caledonia crust above a dipping LVZ						
1	2.8	1.6	2.2	0.5	—	—
2	4.8	2.8	2.5	1.5	—	—
3	6.0	3.6	2.7	23.0	15	15
4	8.1	4.6	3.4	37.0	270	30
5	6.6	3.6	2.9	5.0	270	30
6	8.1	4.4	3.3			
Noumea model						
1	2.8	1.6	2.2	0.5	—	—
2	4.8	2.8	2.5	1.5	—	—
3	6.0	3.6	2.7	24.5	15	15
4	8.1	4.6	3.4	13.0	305	20
5	6.6	3.6	2.9	9.5	305	20
6	8.1	4.6	3.4	11.0	275	30
7	6.6	3.6	2.9	5.0	275	30
8	8.1	4.4	3.3	—	—	—

Some events have short epicentral distance and might contain several incident phases. The 1980 February 18 deep Tongan event displayed in Fig. 4 is typical of what we have collected from this region. For these deep events, a reflected phase from a 650 km mantle discontinuity will arrive at NOU with an apparent velociy very close to, if not the same as that of the direct P-wave. The deconvolution will remove this phase as if it is part of the incident source function. This is not true for the 1972 November 21 deep Kermadec event that has a larger ray parameter. The deconvolution was poor, probably due to different phase velocities invalidating the assumption of one incident angle.

Fig. 9 shows deconvolved radial components which show a good consistency in wave shape. Two prominent arrivals are particularly well correlated from trace to trace. First, a positive phase and later a strong negative phase arriving at 3 s and around 6 or 7 s after the direct P-vave, respectively. From its timing and according to previous Moho depth determination (Collot *et al.* 1982; Dubois 1971), the positive phase around 3 s is interpreted to be the P-to-S conversion at the Moho discontinuity from 25 to 30 km in depth, depending on crustal velocities. From the record section, one can see that the timing of the negative phase has a quite noticeable variation with back-azimuth and decreases from north to south by about 1.5 s. This variation is far above the reading accuracy of the phase and cannot be explained by ray parameter variation. It is very unlikely that such an azimuthally well distributed phase would be P-to-surface wave conversions on rapid interface topographic variations, so we interpret it as a simple P-to-S conversion at a deep dipping interface from a low to a higher velocity medium as shown on Fig. 7.

To test this interpretation, we have compared observed relative arrival times for that phase with computed ones for a simple model (Table 2, model 1) with a dipping LVZ, yielding a minimum variance for a varying strike and a varying depth of this layer. For each depth, the strike of the LVZ is incrementally varied from 0° to 360°. Fig. 10 displays the strike direction and the residual variance curves as a function of the depth of the top of the LVZ, for several dips of the LVZ. The value of the strike around the depth for which the residual variance curves have their minima, is well constrained to 270° ± 5°. Moreover, this value is quite stable at depths shallower than 65 km for any dip. The depth for which the variance is minimized, does not vary more than 1 km when the dip varies from 16° to 28°. Of course this depth around 60 km is model-dependent and can be decreased by several kilometres with a slower model. By repeating this procedure for different Moho dips and strikes, the results lead to very similar strike directions for the LVZ.

After the geometry of deep layers is constrained by the

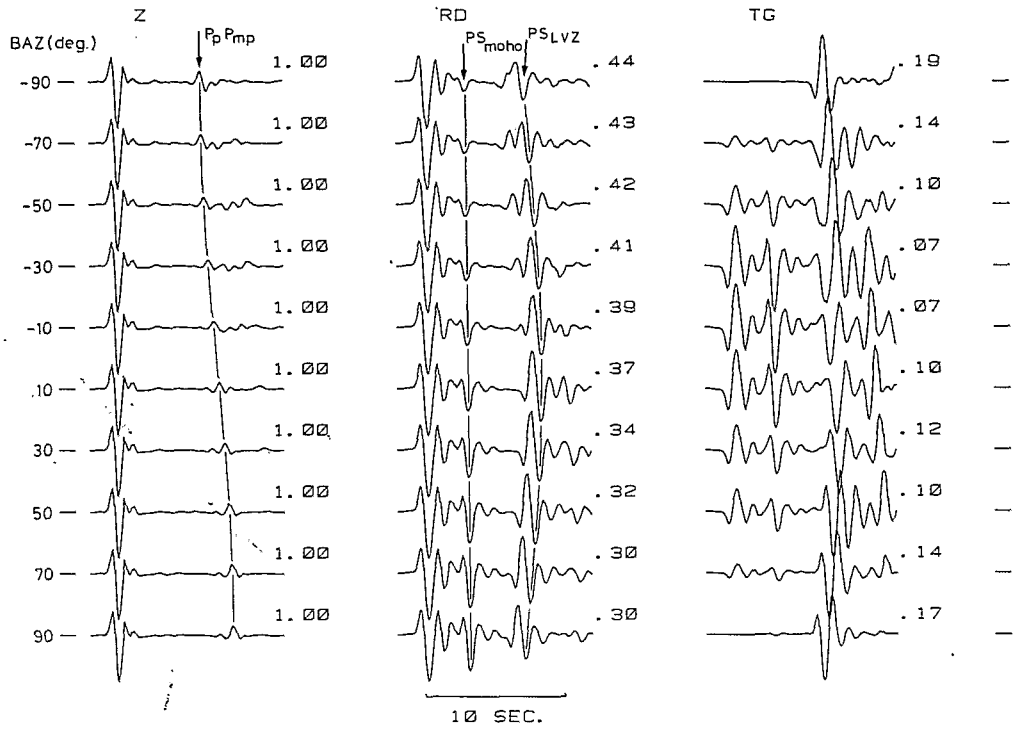

Figure 7. Synthetic seismograms for the model 1 (Table 2) for a back azimuth varying from −90° to 90°. The computational parameters are the same as in Fig. 6. Major phases examined in this study are indicated by arrows. *PS* is the *P*-to-*S* conversion at an interface in the model, and P_pP_{mp} is the first order reverberation in the crust.

radial component, we check whether the polarities of the tangential components are in agreement with this solution. Fig. 11 shows a polar plot of sign change of the two interpreted *P*-to-*S* converted phases at both interfaces bounding the LVZ, between the radial and the tangential components. As before, a plus sign means the same polarity on the two horizontal components, a minus sign, an opposite polarity between them. Only the observations made from clear tangential phases are reported, allowing unambiguous reading of polarity. The deconvolved radial and tangential components are shown around the plot. The first seconds of the 1974 September 7 event have also been plotted to show the Moho P_s on both horizontal components for that particular back-azimuth. This will be useful for determining the Moho orientation. The rest of these particular deconvolved traces are confusing due to a complex incident source function. There is a change of polarity between N 1° and N 85°, defining a wide range of possible dip direction. This result is in agreement with the previous northward dip orientation found from relative travel-time solutions which fall in this range. The eastward tangential first motion solution is slightly out of this range and reflects the complexity of the underlying structure which must include different dip orientation. The Moho interface itself must have a dip which could be oriented northeastward (Dubois 1971), perpendicular to the NW trend of New Caledonia, to take into account the thickening of the crust under the central mountain chain due to a root effect.

To constrain more accurately the depth, dip and strike to the Moho and the LVZ, we used our first model (Table 2, model 1) for modelling the observed data. This model was derived taking into account all the available data for the area under study. The densities and the seismic velocities of the first two sedimentary layers were extrapolated from Collot *et al.* (1982) and Shor, Kirk & Menard (1971). Those parameters of the first layer are appropriate for the material underlying the station which is of flysch type, frequently found in upper sedimentary layers in oceanic active margin areas. Almost the whole crust is represented by a single layer with density and thickness very close to those found by Collot *et al.* (1982). This representation is obviously not realistic, but it will be efficient enough to model the observed data for which, as we can see on Fig. 9, there is no important phase before what we interpret as the Moho P_s-wave. This crustal model remained the same in our modelling procedure. Only seismic refraction studies would be able to give a more precise velocity structure as done, for example, on Mauna Loa volcano by Zucca *et al.* (1980). The LVZ and the bordering velocities have been chosen in order to produce strong P_s phases, a negative one at the top of this layer followed by a positive one at the bottom, as it is often observed on radial data (Figs 9 and 11).

Using a trial and error procedure, a search has been made for a good fit to the observed tangential component which is highly sensitive to variation in the model. Moho strike has been found to lie between N 10° and N 20° with a dip between 15° and 20° and the Moho depth between 25 and 27 km. Synthetics computed with this model were compared to the data and are displayed on Fig. 12 for three different back-azimuths and for several Moho depth. The Moho depth is found both by adjusting the direct P_s converted phase and the reverberated phases in the crust with observed seismograms. A trade-off has been observed

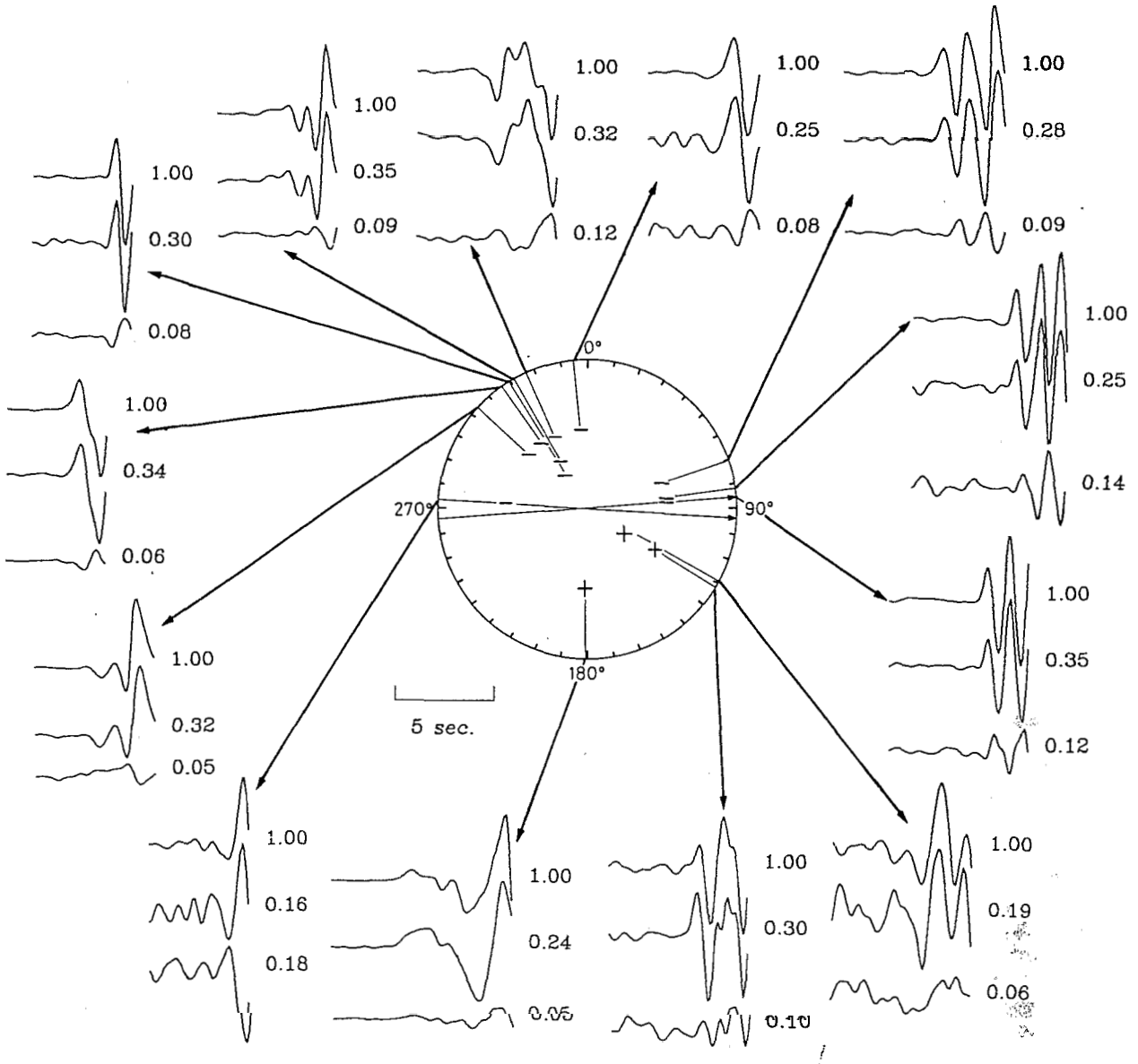

Figure 8. Polar plot of the observed horizontal components of first motion versus back-azimuth for 13 earthquakes. For each event, the traces are, from the top, the vertical, radial and tangential components of ground motion. The sign + or − indicates that if both components have the same polarity or an opposite polarity, respectively. The distance to the center has no significance. The dip direction is eastward as shown by the solid arrows.

between depth and dip that gives an uncertainty of 2 km on Moho depth determination if the same dip is conserved for all the data. The crustal shear velocities are then quite well constrained by the timing of the reverberations and correspond to an average Poisson ration of 0.22, a reasonable value for the crust. These synthetics were computed only for events whose bounce points at the free surface of reflected rays are onland in New Caledonia. For seaside coming events, reverberations occur offshore and then would not be adequately computed with models without a water layer and oceanic crust. Even in the examples presented, important near-surface effect differences remain between the NNW coming events and the east coming event whose first multiples in the crust have their bounce points in metamorphic or sedimentary sequence of the west coast and in the ophiolite nappe east of Noumea, respectively.

With an average crustal thickness of 26 km, two important phases, the P_pP_{mp} and P_pP_{ms}, interfere with the direct P_s phases from the LVZ. This effect is principally visible on the tangential component where the reverberated phases are as large as the direct converted phases. This interference makes the reading of polarities uncertain. This is why only part of the data have been used on Fig. 11 for constraining the dip direction of the LVZ.

If the converted phases identified on Fig. 9 are correctly reproduced on both horizontal components, several large amplitudes are not fitted by the synthetics. Most of these unmatched phases are later than the *PS* Moho phase. The corresponding nearly flat portion on the synthetics is due to the homogeneous 37 km thick layer between the crust and the deep LVZ, which is a very unlikely structure. We found that a straightforward way to model the large unfitted amplitudes has been to synthesize extra P_s phases generated

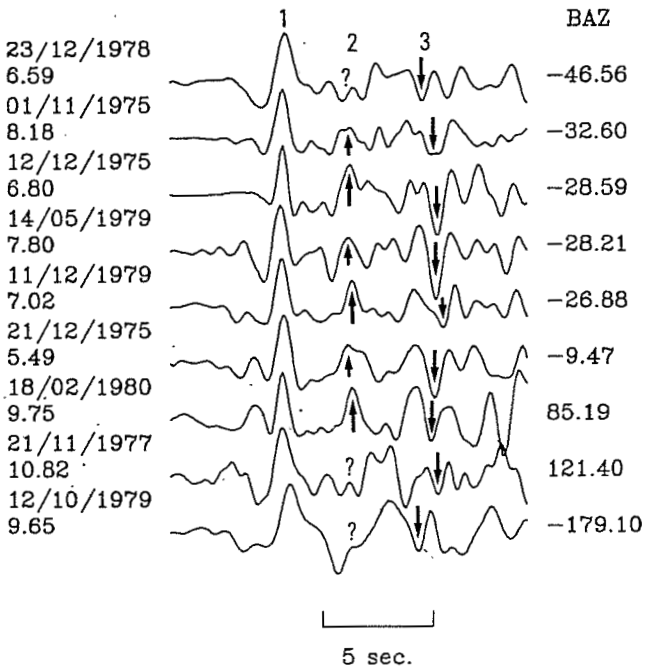

Figure 9. Deconvolved radial P waveforms. Arrows indicate interpreted arrivals: 1 is the direct P wave, 2 the P-to-S converted phase on the Moho and 3 the P-to-S converted phase on the top of the LVZ. Note that the radial P_s Moho is impulsive from north–northwest to east back-azimuths and vanishing elsewhere. This crudely corresponds to landside coming event and seaside coming event.

at new velocity contrasts within the upper mantle above the LVZ.

Let us go back to Fig. 9 to notice that the amplitude and the wave shape of the Moho P_s are not constant from trace to trace. This phase has large amplitude for events coming with NNW to NE back-azimuth while it vanishes for the S and SE coming events. In that case it is followed by large amplitudes which are not presented when the Moho P_s is important. Those observations suggest that the Moho interface presents important thickness variations and would be a broader transition zone southward. In addition, we can see on Fig. 11 that the 1974 September 7 event coming from the west, argues against the previous solution for the Moho dip direction. Its tangential P_s Moho

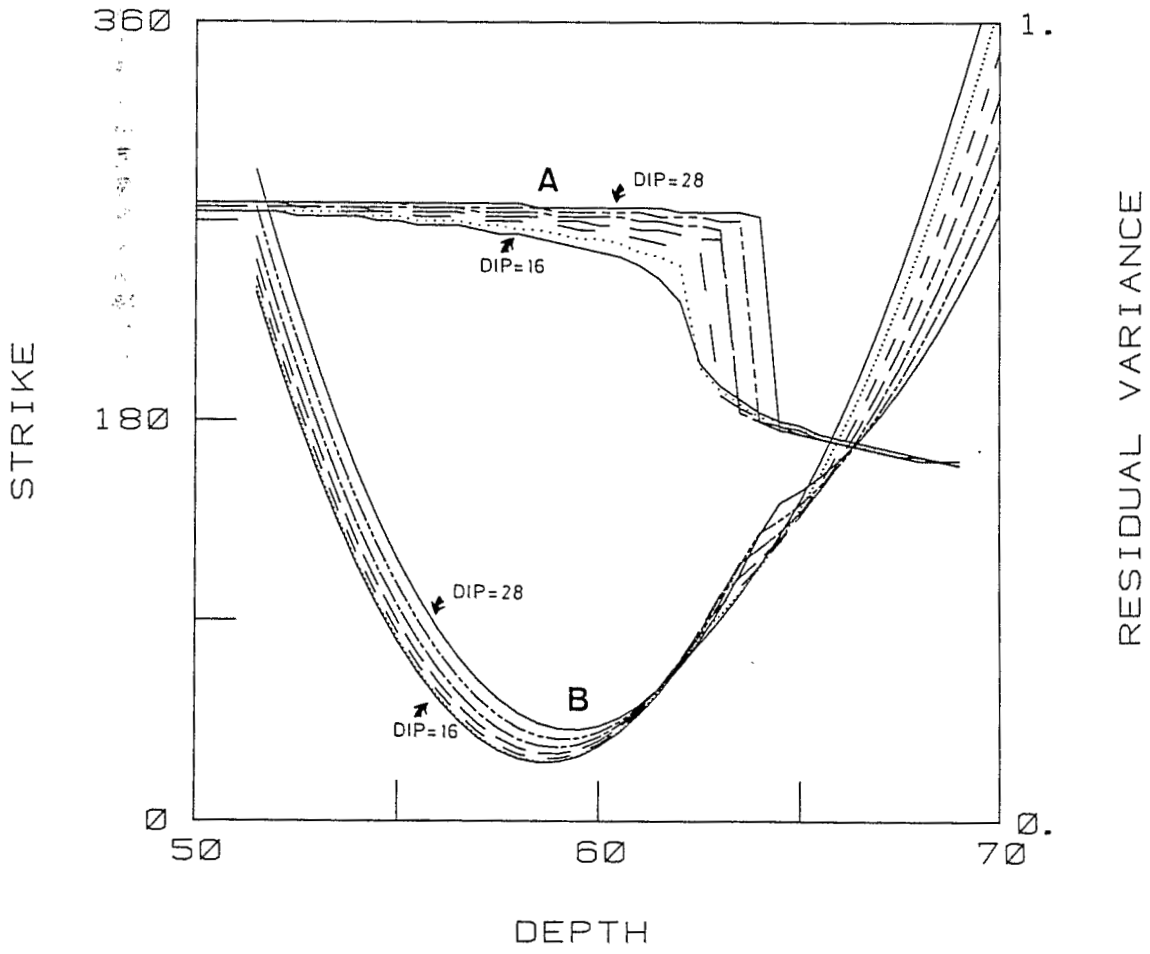

Figure 10. Least-squares inversion results to estimate the strike direction of the LVZ from the relative arrival times of the P-to-S converted wave at the top of the LVZ, shown by arrows on Fig. 9. The dip of the LVZ is incremented by 2° steps from 16° to 28°. Strike curves (group A) are read on the left scale, residual variance curves (group B) on the right scale. See text for details.

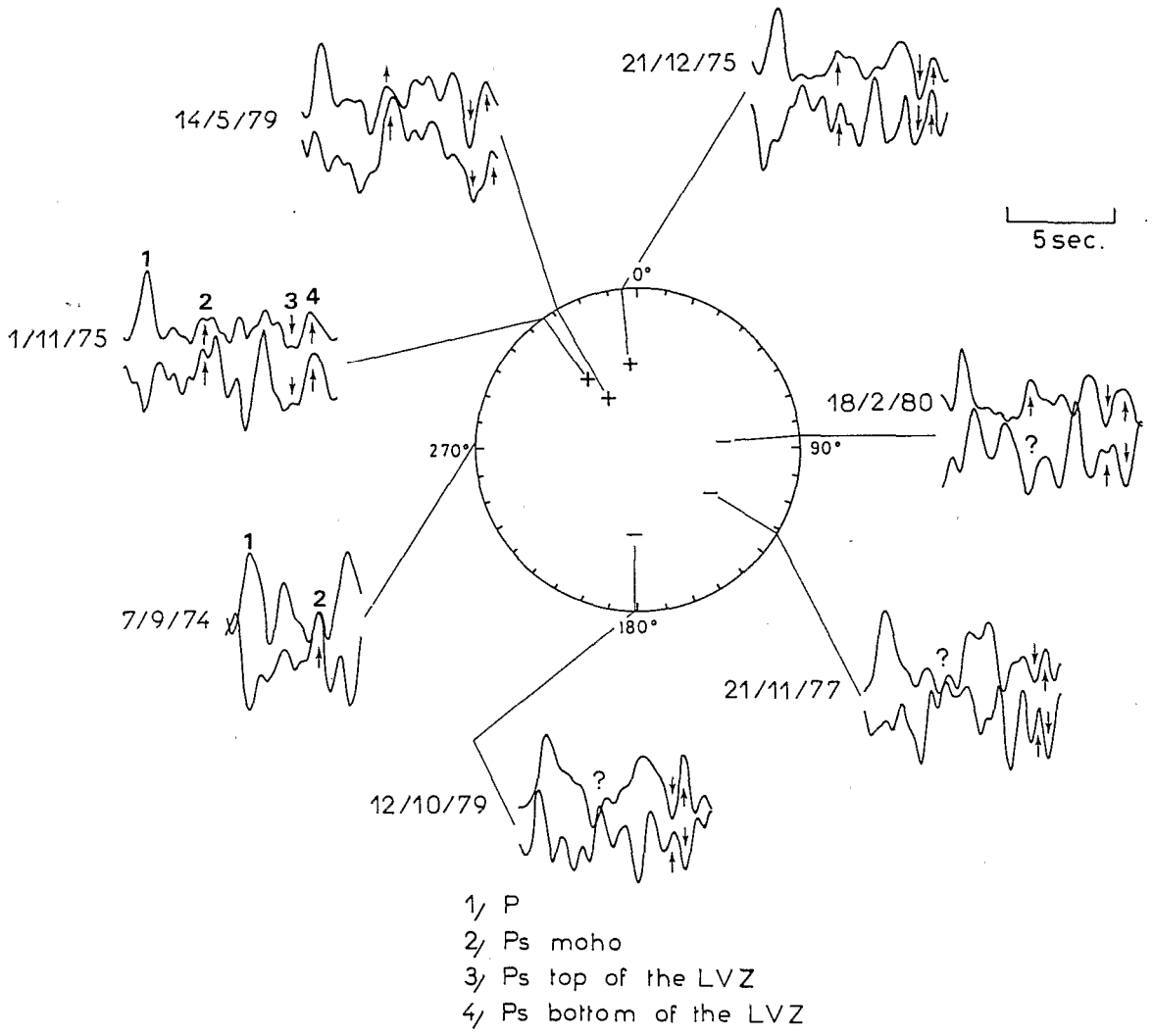

Figure 11. Polar plot of the deconvolved radial (top trace) and tangential components (bottom trace) versus back-azimuth for seven earthquakes. Arrows indicate the polarity of some interpreted P_s phases. At the end of each trace, except for the 1974 July 9 event, the two phases with opposite polarity are interpreted to be the converted phases at the top and at the bottom of the LVZ. The sign convention for the polarity change of these phases between the two horizontal components is the same as for Fig. 8. From this plot, the possible LVZ dip directions are located in the north-eastern quadrant.

is positive and very strong and neither its amplitude nor polarity can be explained by a N 110° dipping Moho. It suggests more a northward dipping Moho. A possible topography for producing these waveforms could be a curved Moho interface, slightly northward dipping offshore like the deep LVZ, changing abruptly to an eastward dip when moving from the W coast toward the E coast.

Fig. 13 shows the equalized data for the three previous events plus another with synthetics computed for the final model (Table 2, model 2). In this model, new velocity discontinuities have been added within the wedge of upper mantle above the deep LVZ to set up new converted and reverberated phases for fitting the unmatched observed phases in the previous modelling. Interface geometry has been adjusted as above through waveform fitting of both horizontal components. Again, we found, by observing polarity changes on the tangential component between events coming from the N and from the E, that the strikes of those new layers are in the NW quadrant. The dip angles in this transition zone have been estimated to be between those of the Moho and of the deep LVZ. For each event, we have looked for the best fit that produced fluctuations in the model in the depth of some interfaces. This practice has been necessary in modelling the tangential component. Indeed many reverberated phases, which are much more sensitive to depth than the direct phase, are actually present and control the tangential component waveform. Nevertheless the model remains geologically unchanged by the small variations that, in fact, allow the determination of depths with a maximum standard deviation less than ±2 km. The errors have been computed from the differences between the models used to compute the synthetics shown in Fig. 13.

The final model with error bars on depth of interfaces is displayed in Fig. 14. In this model, all the major phases are well fitted with the right polarities on the tangential component. Most of the relative amplitudes of the tangential synthetics are also very close to the observed

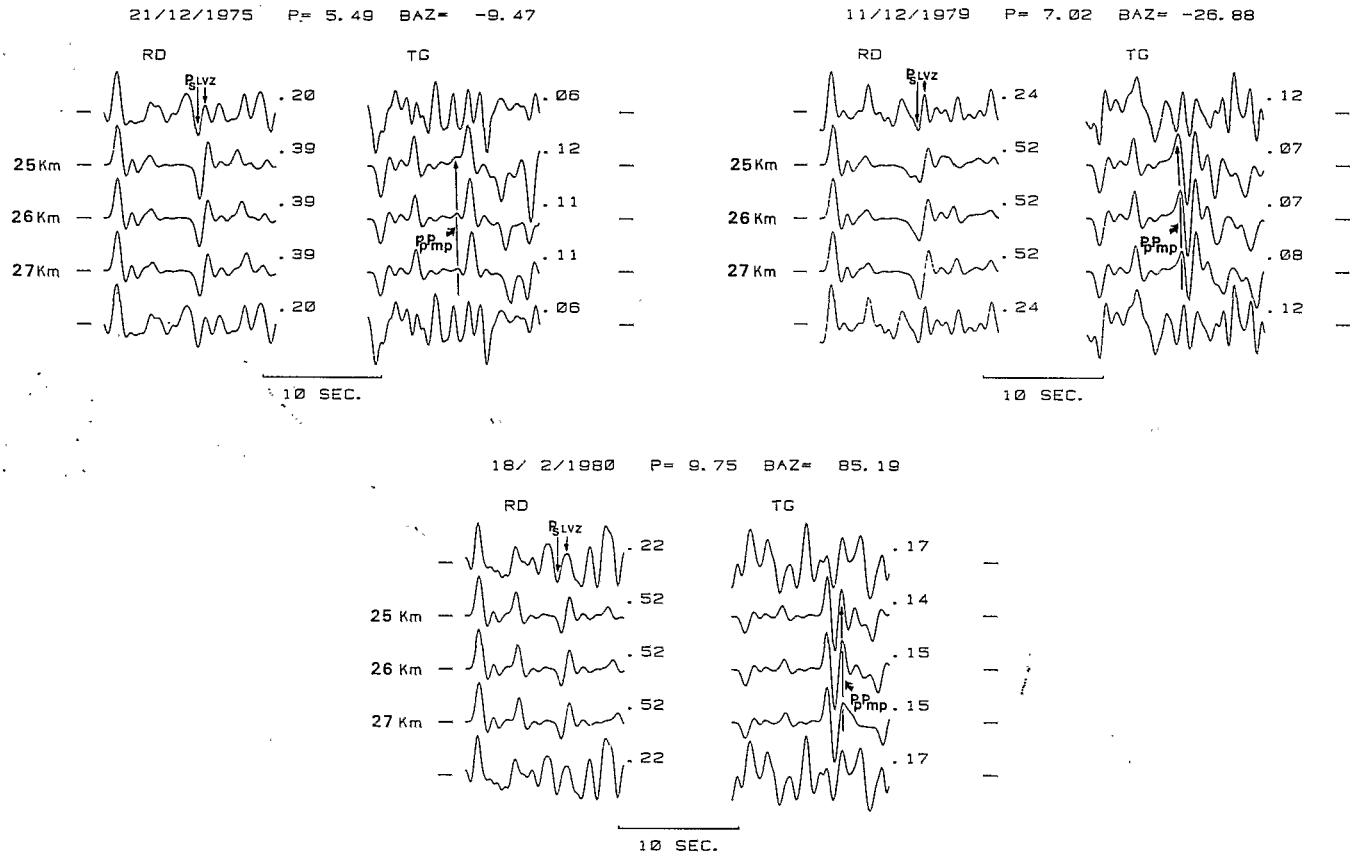

Figure 12. Deconvolved radial and tangential data (first and lowest traces in each event modelling) are compared to synthetics (intermediate traces) calculated with model 1 (Table 2) for several depths to Moho discontinuity. The dashed line on the tangential component shows the computed P_pP_{mp} phase interfering with the P-to-S converted phase group from the LVZ. This may lead to misreading of some converted phases polarity.

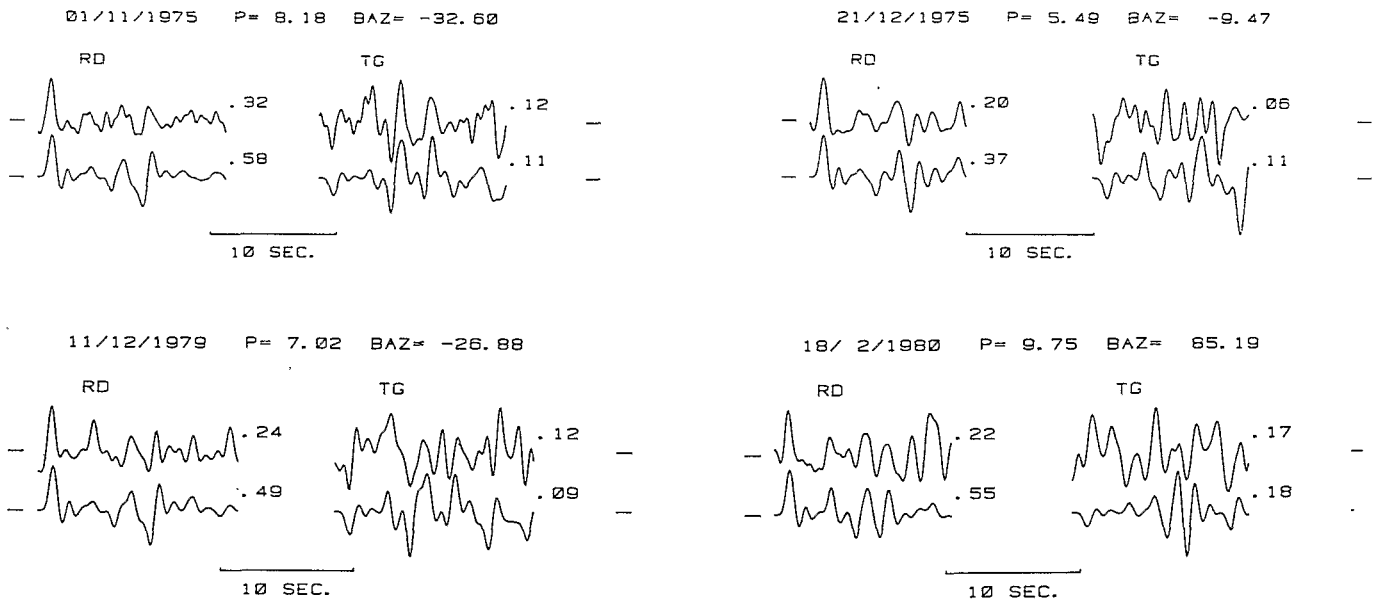

Figure 13. Comparison of observed (top) and synthetic (below) seismograms calculated with the final model (Table 2, model 2).

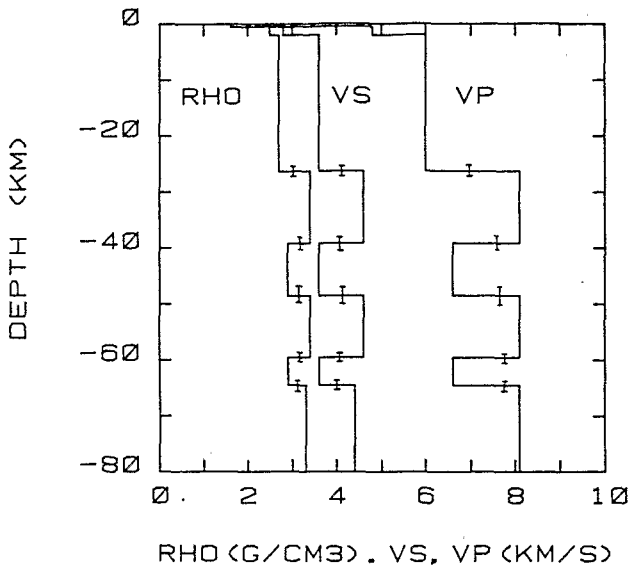

Figure 14. NOU model with error bars.

ones. This is not true, however, for the radial component for which the data have smaller relative amplitudes in all cases.

The transition zone is a very complex zone to model because its effect on the data is not similar from trace to trace. Much more data would be necessary to resolve this structure. Although the propagation of teleseismic body waves is nearly vertical below the station, the places of *P*-to-*S* conversion at LVZ interfaces or at the deepest transition zone interfaces may be separated by several tens of kilometers for opposite back-azimuths. For the 1975 November 1 event, the conversion at the top of the LVZ, computed with the final model, is at 12 km in a N 95° direction from the station, while it is at 22 km in a N 135° direction for the 1982 February 18 event. In each case, note the large azimuth anomaly of respectively 63° and −50°. The two places of conversion are then separated by 32 km. The ray paths in the above complex transition zone are also separated by the same distance and can encounter different melange-like zones. Recent deep seismic reflection profiles in ancient convergence zones, such as the Winch profile of BIRPS (Brewer & Smythe 1986) or the 'Nord de France' profile of ECORS (Cazes *et al.* 1986), show that this distance is large enough to observe drastic lithologic variation in the crust or the upper mantle. For the wavelength of about 6 km used in this study, body wave propagation in such a rapidly varying structure can be variously affected as a function of back-azimuth and ray parameter. Undoubtedly, this zone includes many more than the few layers proposed in the model. But this kind of structure cannot be resolved by the wavelength used in this study and it is not nearly as well constrained as the other main features of the model. Unfortunately, this zone has an especially great effect on the tangential component and controls its waveform in the 5–7 s range after the direct *P*-wave. Reverberations in both modes within those layers, weakly present on the radial component, must also add to the complexity of the whole tangential component. As an example, the first few seconds of all our tangential components are very complicated compared to the very quiet waveform of the equivalent portion on the radial components.

However, layered models cannot account for all propagation effects present in the data. Waveform complexity can arise from several other causes such as scattered energy and anisotropy. Anisotropy could be checked by looking at the *S*-wave splitting in the *S*-wave arrival. Although it is likely that anisotropic materials are present in the wedge above the deep LVZ (Ando, Ishikawa & Yamazaki 1983), this effect cannot be measured using the major *P*-to-*S* converted waves of the *P* coda used in this study. As we observe significant tangential first motion, this effect must not be the major one because *P*-wave propagation in a flat layered anisotropic medium does not generate that phase on the tangential component (Keith & Crampin 1977). There might also be scattered energy present in the data, as vertical *P*-coda amplitudes are comparable to the radial ones (Fig. 3). The latter phases in the coda have not been successfully computed with our model and the lack of coherence from one coda to another suggests the presence in these waveforms of scattered surface waves. The final model certainly shows a simple version of the actual interface geometry and it is only valid for the structure within 25 km from NOU. It would be very difficult to constrain some of its parameters further with the available data set. It is clear that such an analysis falls short if the structure has too rapid a variation of some of its parameters over the area of investigation, as seems to be the case for the transition zone. In contrast, the deep LVZ has been identified in most of the data, and its interpretation is more straightforward.

A MODEL FOR THE NOUMEA AREA

Modelling of the site response of NOU has provided some fundamental information about the upper mantle structure beneath New Caledonia. Waveforms presented here clearly show that: (i) high velocity contrasts from a velocity inversion exist at a depth of about 60 km and present strong lateral variation inferred from the tangential component of motion. From both travel times and waveform modelling, these structures have been found to dip northward at least 20°; (ii) the Moho depth is 26 ± 1 km and the crust has mean compressional and shear velocities of 6 and 3.6 km s^{-1}, respectively. Azimuthal coverage has shown that the *PS* Moho phase is impulsive and well developed for landside coming events while it is complex and vanishing for seaside events; and (iii) the wedge of upper mantle below the crust is largely heterogeneous again with a velocity inversion dipping northeastward.

All these observations strongly suggest that a major zone of intralithospheric thrusting is present beneath the southern part of New Caledonia. Fig. 15 is a N–S cross section positioned on NOU, with the offshore structures from Shor *et al.* (1971) and the proposed model below the west coast of New Caledonia. We propose that the oceanic layers obtained from offshore refraction profiles N 9 and N 10 and the low-velocity zone at a 60 km depth beneath NOU are the same geological unit, a large zone of thrusting, defined by connecting those two points. The resulting dip is about 30° with a straight line connection and

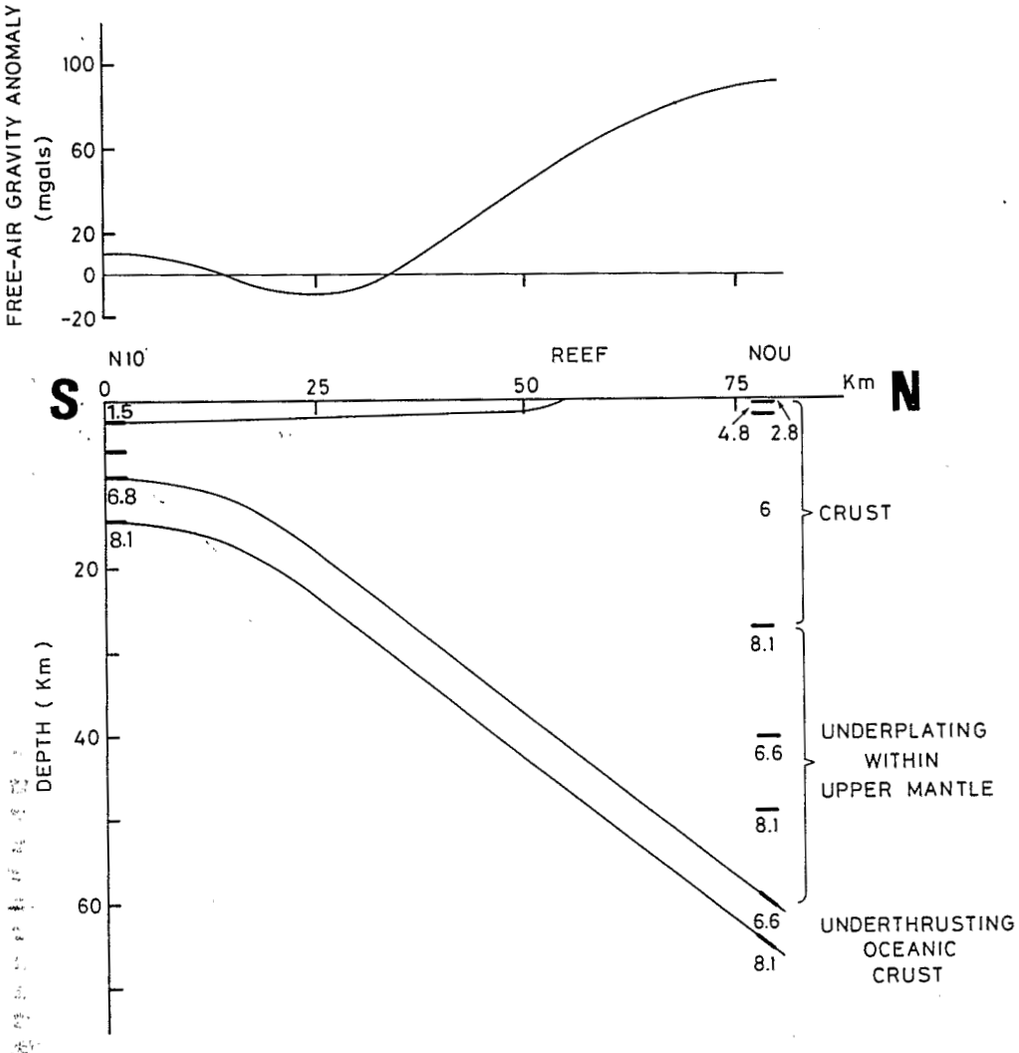

Figure 15. Shematic cross section (below) of a north–south profile including NOU structure. N 10° structure taken from Shor *et al.* (1971). On top is displayed the free-air gravity anomaly along the profile.

is slightly increased with a curved interface, depending on the bending of the New Caledonia basin lithosphere. The Moho depth N 9 is determined to be 1.4 km deeper than at N 10 (Fig. 2) which is closer to New Caledonia. Projecting this NW-oriented refraction line N 9–N 10 in the N–S cross-section gives a dip angle of only 1.5° between the two refraction stations separated by 51 km. Considering then a flat Moho from the projection of the N 10° refraction station, the dip of the inferred thrust zone is 40° below NOU with a curved contact between the two plates. These two values give a range of dip fully compatible with the 30° dip of our model required for matching tangential amplitudes.

The complicated waveforms of the seaside coming events may reflect the complexity of the thrust zone. The Moho well-defined by a sharp boundary elsewhere, should look more and more like a sheared and laminated boundary toward the thrust zone. As observed in the data, this type of crust-mantle boundary is expected to produce weak and complicated signals. The underlying transition zone may largely consist of mantle-like material with slivers of crustal material. These anomalous zones of low velocity could be a melange-like region made of subducted or underthrusted sediments and oceanic rock. Note that this model of a major thrust contact, including a zone of underplating above a dipping crust, is similar to the structure across the Juan de Fuca subduction zone found by Spence, Clowes & Ellis (1985) whose final model above Vancouver Island also includes two velocity inversions.

On Fig. 15 the gravity anomaly across the west coast, constructed from the gravity anomaly map of Collot *et al.* (1982), is also plotted. The New Caledonia basin low is present all along the west coast and reaches −80 mgals northwestward. This negative gravity anomaly, which is independent of the bathymetry, could be a consequence of the major thrust zone as commonly observed in a subduction zone. Cazenave, Rosemberg-Borot & Robinowicz (1986) have shown that the location of the gravity low in an arc-trench system is not always above the trench and could be shifted toward the inner slope of the trench due to the presence of large accumulation of low density material. In our case there is no apparent trace of a trench which

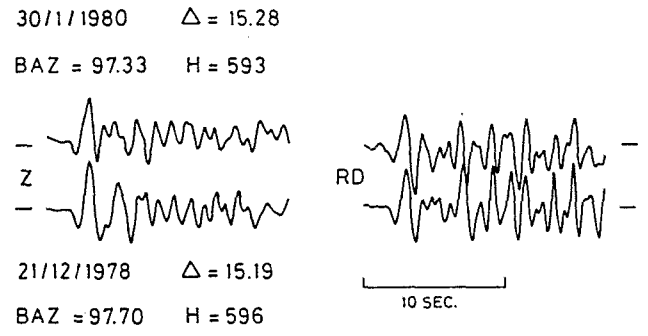

Figure 16. Example of vertical and radial *P* waveform of deep events of the Tonga subduction zone recorded a KOU (Fig. 2).

could have been filled up by the important post-obduction sedimentation, and the gravity low would be above the maximum thickness of sediment.

In order to check our interpretation of the NOU data and to extend our conclusions to the whole island, we have collected few data recorded at KOU (Fig. 2), a two-component station (E and W–W) with approximately the same instrumental response as at NOU. Fig. 16 shows two deep earthquakes of the Tonga subduction zone which are naturally rotated into the radial component of motion at KOU station. Despite a waveform on the vertical component quite different between the two events, the two radial components are similar and exhibit a succession of very large negative and positive phases from 4 to 9 s after the direct *P*-wave. These relative arrival times correspond to those observed at NOU for the *P*-to-*S* conversions at the different height velocity contrasts present under the station. They might possibly reveal, by performing an appropriate 3-D data analysis, a northern extension of the thrust contact found south of New Caledonia. This data is part of an ongoing study on the New Caledonia and Loyalty island structures for which we are now operating three-component stations.

DISCUSSION AND CONCLUSION

Many authors have suggested the presence of a subduction zone in the New Caledonia area (e.g. Lapouille & Dugas 1975; Paris & Lille 1977; Parrot & Dugas 1980; Kroenke 1984). Dubois *et al.* (1973, 1974) first proposed a northeastward dipping subduction zone with a trench located west of New Caledonia at the place of the gravity anomaly minimum (Collet *et al.* 1982). A major requirement for a subduction zone is that it should produce a volcanic arc. As no arc is apparent, an important point to elucidate when searching for it in this area, is the occurrence time of the supposed subduction in relation to the time of the obduction (Paris 1980). According to the model of Collot *et al.* (1982), the latter could have shortened the west Loyalty basin by at least 80 km. Assuming that the Loyalty ridge, interpreted by Dubois *et al.* (1974) as the missing volcanic arc, existed in the Eocene before the obduction phase, it was then distant from the inferred trench by 280–340 km for a southwestward, i.e. perpendicular to the New Caledonia axis, to a purely southward direction of obduction motion. With at least a 110 km depth reached by the subducted plate for the occurrence of the volcanic front (Tatsumi 1986), this large arc–trench separation would imply quite a low angle of subduction (less than 20°) for a N to NE dipping subduction zone. This value, together with the presence of the well-developed west Loyalty oceanic basin (Pontoise *et al.* 1982; Bitoun & Recy 1982) in front of the Loyalty ridge, make the interpretation of Dubois *et al.* (1974) unlikely. If an arc existed before the obduction phase with the aforementioned related trench location, we must look for it closer to the New Caledonia area, approximately at the place where the rooted ultramafic now continuously overlies the east margin of the island. Then, as proposed by Kroenke (1984), the large low-density mass underlying the ophiolite off the east coast in the Collot *et al.* (1982) model could represent a buried volcanic arc. However, despite years of geological field work, very few traces of calc-alkaline volcanic activity have been found in New Caledonia. This makes the existence of a volcanic front close to the island still questionable. The deep reflectors found beneath the Noumea area indicate the trace of a thrust fault as well as the presence of an old subduction zone. This problem will remain open pending a systematic search for volcanogenic components in the Eocene flysch of the west coast.

Furthermore, we know from Paris (1981) that no major compressional tectonic event has been recorded in either the continuous sedimentation along the west coast from the late Cretaceous opening of the New Caledonia basin—when New Caledonia island separated from Gondwanaland—until the upper obduction, or in the ophiolite nappe from the obduction up to recent time. Therefore, the most likely time for large thrust motion along the west coast is during the obduction phase as a syntectonic event. This could be the consequence of underthrusting and overthrusting occurring together along opposite shear zones (Fig. 17).

If obduction is generally initiated at a pre-existing contact or zone of weakness such as a plate boundary (Michard, Juteau & Whitechurch 1985; Nicolas & Le Pichon 1980; Coleman 1981; Dewey 1976), then the obduction of the Loyalty basin lithosphere could have begun at a major intralithospheric thrust contact within the proto-Loyalty basin or at a subduction zone with its related trench located east of New Caledonia. The thrust motion could have occurred over the island when the latter tried to subduct. In this case, New Caledonia obduction is an example of obduction linked to the subduction of continental crust (Moores 1970; Davies & Smith 1971). The west coast underthrusting could have begun simultaneously at a weak zone along the west margin of New Caledonia in response to compressive stress not completely absorbed by the obduction process.

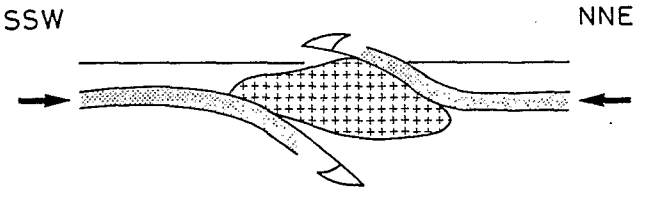

Figure 17. Diagramatic strain pattern for the late Eocene tectonic in New Caledonia region. The crossed area represents the continental core of the island and the dotted areas are oceanic crust.

In that model, the nearby Loyalty islands could be the related volcanic front of a north-northeastward dipping subduction zone with its related trench within the proto-Loyalty basin, as suggested by the southwestward direction of obduction motion. The Loyalty ridge seems to be superimposed on the North Loyalty basin, trending perpendicularly to the Eocene (42–56 Myr, Weissel, Watts & Lapouille, 1982) magnetic lineations of this marginal basin. In that condition, the Loyalty subduction could have been active in the upper Eocene up to the obduction phase. This age for the building of the Loyalty ridge is not in agreement with the Late Miocene basalt (10 Myr, Baubron, Guillon & Recy 1976) exposed on Mare island. These samples have an alkaline composition and would likely represent a secondary phase of volcanism without relationship to the older tectonic event responsible for the Loyalty ridge formation.

In conclusion, we have found geophysical evidence for an inactive northward dipping structure up to 65 km deep under the southern part of the New Caledonia island. This structure could be described in terms of a subduction zone, but no definite proof exists to confirm this hypothesis. However, some authors propose subduction along the west coast of New Caledonia (Kroenke 1984), which would have been active from the Upper Cretaceous until the Late Eocene obduction (Collot *et al.* 1987). This scheme is mainly based on very few arc-volcanic samples of unknown age found on the island (Paris 1981; Collot *et al.* 1987). Moreover, Kroenke (1984) suggests that no subduction occurred along the western edge of the N–S trending Norfolk ridge (Fig. 1). In that case, the model of Collot *et al.* (1987) should imply a large width difference between the northern part of the New Caledonia basin, west of New Caledonia, and the southern part. This is not observed (Fig. 1); the width of the New Caledonia basin remains almost constant from N to S. Consequently, we suggest that the west coast underthrusting, which perhaps reaches the early stages of subduction, and the east coast obduction are contemporaneous and are both the consequences of Late Eocene plate convergence in the New Caledonia area.

ACKNOWLEDGMENTS

This work was supported by the Institut Français de Recherche Scientifique Pour le Développement en Coopération (ORSTOM). We thank M. Cara, C. Langston, J. Dorman and L. Kanter for their helpful comments and their critical review of the manuscript. B. Pelletier is acknowledged for many enlightening discussions about the tectonics of New Caledonia. We are grateful to C. Baldassary and R. Decourt for their valuable maintenance of the NOU station.

REFERENCES

Aki, K. & Richard, P. G., 1980. *Quantitative Seismology,* ed. Freeman, San Francisco, CA.

Ando, M., Ishikawa, Y. & Yamazaki, F., 1983. Shear wave polarization anisotropy in the upper Mantle beneath Honshu, Japan, *J. geophys. Res.*, **88,** 5850–5864.

Avias, J., 1967. Overthrust structure of the main ultrabasic New Caledonian massives, *Tectonophys.*, **4,** 531–541.

Baubron, J. C., Guillon, J. H. & Recy, J., 1976. Géochronologie par la méthode K/Ar du substrat volcanique di l'ile de Maré, archipèl des Loyauté (Sud-Ouest Pacifique), *Bull. Bur. Rec. Geol. Min.*, **2,** IV, 3, 165–176.

Bitoun, G. & Recy, J., 1982. Origine et évolution du bassin des Loyauté et de ses bordures après la mise en place de la série ophiolotique de la Nouvelle Caledonie, in *Equipe de Géologie-Géophysique du centre ORSTOM de Noumea,* Contribution a l'étude du Sud-Ouest Pacifique, travaux et documents de l'ORSTOM No 147, 505–539.

Blake, M. C., Brothers, R. N. & Lanphere, M. A., 1977. Radiometric ages of blueschists in New Caledonia, *Int. Symp. Geodynamics of the Southwestern Pacific,* pp. 279–281, ed. Noumea, Technip, Paris.

Bowin, C., Lu, R. S., Lee, C. S. & Schouten, H., 1978. Plate convergence and accretion in Taiwan–Luzon region, *Bull. Am. Ass. Petrol. Geol.*, **62,** 1645–1672.

Brewer, J. A. & Smythe, D. K., 1986. Deep structure of the foreland to the Caledonian orogen, NW Scotland: results of the BIRPS WINCH profile, *Tectonics,* **5,** 171–194.

Brudick, L. J. & Langston, C. A., 1977. Modelling crustal structure through the use of converted phases in the teleseismic body-waveforms, *Bull seism. Soc. Am.*, **67,** 677–691.

Cazenave, A., Rosemberg-Borot, C. & Rabinowicz, M., 1986. Geoid lows over deep-sea trenches, *J. geophys. Res.*, **91,** 1989–2993.

Cazes, M., Mascle, A., Torreilles, X., Bois, Ch., Damotte, X., Matte, Ph., Raoult, X., Pham, V. N., Hirn, A. & Galdeano, X., 1986. Large variscan overthrust beneath the Paris basin, *Nature,* **323,** 144–147.

Choy, G. L. & Richard, P. G., 1975. Pulse distortion and hilbert transformation in multiply reflected and refracted body waves, *Bull. seism. Soc. Am.*, **65,** 55–70.

Coleman, R. G., 1971. Plate tectonic emplacement of upper mantle periodotites along continental edges, *J. geophys. Res.*, **76,** 1212–1222.

Coleman, R. G., 1981. Tectonic setting for ophiolite obduction in Oman, *J. geophys. Res.*, **86,** 2497–2508.

Collot, J. Y., Missegue, F. & Malahoff, A., 1982. Anomalies gravimetriques et structure de la croute dans la région de la Nouvelle Calédonie: enracinement des péridotites, in Equipe de Géophysique du centre ORSTOM de Noumea. Contribution a l'étude du Sud-Ouest Pacifique. Travaux et documents de l'ORSTOM No 147, 549–564.

Collot, J. Y., Malahoff, A., Recy, J., Latham, G. & Missegue, F., 1987. Overthrust emplacement of New Caledonia ophiolite: geophysical evidence, *Tectonics,* **6,** 215–232.

Davies, H. L. & Smith, I. E., 1971. Geology of Eastern Papua, *Bull. geol. Soc. Am.*, **82,** 2399–3312.

Dewey, J. F., 1976. Ophiolite obduction, *Tectonophys.*, **31,** 93–120.

Dubois, J., 1971. Propagation of *P*-waves and Rayleigh waves in Melanesia: structural implications, *J. geophys. Res.*, **76,** 7217–7240.

Dubois, J., Guillon, J. H., Launay, J., Recy, J. & Trescases, J. J., 1973. Structural and other aspects of the New Caledonia–Norfolk area, in *The Western Pacific: Isand Arcs, Marginal seas, Geochemistry,* pp. 223–235, ed. P. J. Coleman, University of Western Australia Press.

Dubois, J., Ravenne, C., Aubertin, A., Louis, J., Guillaume, R., Launay, J. & Montadert, L., 1974. Continental margins near New Caledonia, in *The Geology of Continental Margin,* pp. 521–535, ed. Burk, C. A. & Drake, C. L., Springer-Verlag, NY.

Dziewonski, A. M. & Anderson, D. L., 1983. Travel times and station corrections for *P* waves at teleseismic distances, *J. geophys. Res.*, **88,** 3295–3314.

Falvey, D. A. & Mutter, J. C., 1981. Regional plate tectonics and the evolution of Australia's passive continental margin, *Bur. Min. Rec. Jl Aust. Geol. Geophys.*, **6,** 1–29.

Hasegewa, H. S., 1971. Crustal transfer ratio of short and long period body waves recorded at Yellowknife, *Bull. seism. Soc. Am.*, **61,** 1303–1320.

Haskell, N. A., 1953. The dispersion of surface waves in multilayered media, *Bull. seism. Soc. Am.*, **43,** 17–34.

Haskell, N. A., 1962. Crustal reflection of plane *P*- and *SV*-waves, *J. geophys. Res.*, **67i,** 4751–4767.

Hayes, D. E. & Ringis, J., 1973. Seafloor spreading in the Tasman Sea, *Nature*, **243**, 454–458.

Hayes, D. E. & Lewis, S. D., 1984. A geophysical study of the Manila trench, Luzon, Phillipines, 1, crustal structure, gravity and regional tectonic evolution, *J. geophys. Res.*, **89**, 9179–9195.

Helmberger, D. & Wiggins, R. A., 1971. Upper mantle structure of mid-western United States, *J. geophys. Res.*, **76**, 3229–3245.

Ibrahim, A. K., Pontoise, B., Latham, G., Larue, M., Chen, T., Isacks, B., Recy, J. & Louat, R., 1980. Structure of the New Hebrides arc-trench system, *J. geophys. Res.*, **85**, 253–266.

Keith, C. M. & Crampin, S., 1977. Seismic body waves in anisotropic media: Synthetic seismograms, *Geophys. J. R. astr. Soc.*, **49**, 225–243.

Kroenke, L. W., 1984. Cenozoic tectonic development of the southwest Pacific, *UN ESCAP, CCOP/SOPAC Tech. Bull.*, **6**, 98 p.

Langston, C. A., 1977a. The effect of planar dipping structure on source and receiver responses for constant ray parameter, *Bull. seism. Soc. Am.*, **67**, 1029–1050.

Langston, C. A., 1977b. Corvallis, Oregon, crustal and upper mantle receiver structure from teleseismic *P* and *S* waves, *Bull. seism. Soc. Am.*, **67**, 713–724.

Langston, C. A., 1979. Structure under Mount Rainier, Washington, inferred from teleseismic body waves, *J. geophys. Res.*, **84**, 4749–4762.

Langston, C. A., 1987. Evidence for the subducting lithosphere under southern Vancouver island and western Oregon from teleseismic *P* wave convertion, *J. geophys. Res.*, **86**, 3857–3866.

Lapouille, A. & Dugas, F., 1975. Geological evolution of New Hebrides and Loyalty areas, in *Proc. First Southwest Pacific Earth Science Symp., Bull. Aust. Soc. explor. Geophys.*, **6**, 52.

Michard, A., Juteau, T. & Whitechurch, H., 1985. L'obduction: revue des modeles et confrontation au cas de l'Oman, *Bull. Soc. Geol. France*, **8**, 189–198.

Missegue, F., 1981. Gravimétrie, carte de la Nouvelle Caledonie au 1:1000000 et notice explicative, in *Atlas de la Nouvelle Caledonie et Dependance*, p. 6, ORSTOM, Paris.

Moores, E. M., 1970. Ultramafics and orogeny with models of the United States cordillera and the tethys, *Nature*, **228**, 801–842.

Nicholas, A. & Le Pichon, X., 1980. Thrusting of young lithosphere in subduction zone with special reference to structure in ophiolotic peridotites, *Earth planet. Sci. Lett.*, **46**, 397–406.

Owen, J. T., Zandt, G. & Taylor, S. R., 1984. Seismic evidence for an ancient rift beneath the Cumberland plateau, Tennessee: a detailed analysis of broadband teleseismic *P* waveforms, *J. geophys. Res.*, **89**, 7783–7795.

Packham, G. H., 1982. Foreward to paper on tectonics of the southwest Pacific region, in The evolution of the India–Pacific plate boundaries, *Tectonophys.*, **87**, 1–10.

Paris, J. P., 1981. Géologie de la Nouvelle Calédonie: un essais de synthèse, Mémoire BRGM No 113, 279 p., 1 carte FT.

Paris, J. P. & Lille, R., 1977. New Caledonia: evolution from permian to miocene. Mapping data and hypotheses about geotectonics. *Int. Symp. Geodynamics in South-West Pacific*, pp. 195–208, ed. Noumea, Technip, Paris.

Parrot, J. F. & Dugas, F., 1980. The disrupted ophiolitic belt of the southwest Pacific: evidence of an eocene subduction zone, *Tectonophys.*, **66**, 349–372.

Pontoise, B., Collot, J. Y., Missegue, F. & Latham, G., 1982. Sismique réfraction dans le bassin des Loyauté résultats et discussion, in Equipe de Géologie-Géophysique du centre ORSTOM de Nouméa. Contribution a l'étude du Sud-Ouest Pacifique. Travaux et documents de l'ORSTOM No 147, 541–548.

Poupinet, G., 1977. Hétérogénéités du manteau terrestre deduites de la propagation des ondes de volume. Implication géodynamique, *Thèse de doctorat ès sciences*, université scientifique et médicale de grenoble.

Romanowicz, B., Cara, M., Fels, J. F. & Rouland, D., 1984. GEOSCOPE: A French initiative in long period, three components, global seismic network. *EOS, Trans. Am. geophys. Un.*, **65**, 753–754.

Shor, G. G., Jr., Kirk, H. K. & Menard, H. W., 1971. Crustal structure of the Melanesian area, *J. geophys. Res.*, **76**, 2562–2586.

Sorrels, G. F., Crowley, J. B. & Veith, K. F., 1971. Methods for computing ray paths in complex geological structures, *Bull. seism. Soc. Am.*, **61**, 27–53.

Spence, G. D., Clowes, R. M. & Ellis, R. M., 1985. Seismic structure across active subduction zone of western Canada, *J. geophys. Res.*, **90**, 6754–6772.

Tatsumi, Y., 1986. Formation of the volcanic front in subduction zones, *Geophys. Res. Lett.*, **13**, 717–720.

Weissel, J. K., Watts, A. B. & Lapouille, A., 1982. Evidence for late paleocene to late eocene seaflore in the southern New Hebrides basin, *Tectonophys.*, **87**, B243–251.

Zucca, J. J., Hill, D. P. & Kovack, R. L., 1982. Crustal structure of Mauna Loa volcano, Hawaii, from seismic refraction and gravity data, *Bull. seism. Soc. Am.*, **72**, 1535–1550.